HHS Public Access

Author manuscript

J Proteome Res. Author manuscript; available in PMC 2023 September 21.

Published in final edited form as:

J Proteome Res. 2023 August 04; 22(8): 2703–2713. doi:10.1021/acs.jproteome.3c00267.

Absolute quantification of photoreceptor outer segment proteins

Nikolai P. Skiba[1,*], **Tylor R. Lewis**[1], **William J. Spencer**[1,#], **Carson M. Castillo**[1], **Andrej Shevchenko**[2], **Vadim Y. Arshavsky**[1,*]

[1]Department of Ophthalmology, Duke University School of Medicine, Durham, NC 27710

[2]Max Planck Institute of Molecular Cell Biology and Genetics, Dresden, Germany 01307

Abstract

Photoreceptor cells generate neuronal signals in response to capturing light. This process, called phototransduction, takes place in a highly specialized outer segment organelle. There are significant discrepancies in the reported amounts of many proteins supporting this process, particularly those of low abundance, which limits our understanding of their molecular organization and function. In this study, we used quantitative mass spectrometry to simultaneously determine the abundances of twenty key structural and functional proteins residing in mouse rod outer segments. We computed the absolute number of molecules of each protein residing within an individual outer segment and the molar ratio amongst all twenty proteins. The molar ratios of proteins comprising three well-characterized constitutive complexes in outer segments differed from the established subunit stoichiometries of these complexes by less than 7%, highlighting the exceptional precision of our quantification. Overall, this study resolves multiple existing discrepancies regarding the outer segment abundances of these proteins, thereby advancing our understanding of how the phototransduction pathway functions as a single, well-coordinated molecular ensemble.

Keywords

vision; retina; photoreceptor; phototransduction; proteomics; absolute protein quantification

Introduction

Rod and cone photoreceptors are retinal neurons which generate electrical signals in response to capturing light. This process, called phototransduction, takes place in the outer segment organelle that contains a stack of membranous “discs” to facilitate efficient light capture. The molecular composition of the outer segment is rather unique and includes a number of functional and structural proteins specialized in supporting phototransduction. Over the past several decades, most of these proteins have been characterized in great detail, which makes phototransduction one of the most robust systems to study the general principles of GPCR signaling and one of the best understood signaling cascades overall [1, 2]. Not surprisingly, the phototransduction cascade has been the subject of extensive

[*]Send correspondence to Nikolai Skiba at nikolai.skiba@duke.edu or Vadim Arshavsky at vadim.arshavsky@duke.edu.
[#]Current address: Department of Ophthalmology and Visual Sciences, SUNY Upstate Medical University, Syracuse, NY 13210

computational modeling and is viewed as a powerful quantitative system for appreciating the coordination of individual proteins within a complex network (e.g., [3–7]). However, a complete quantitative understanding of phototransduction is still limited by insufficient information on the precise outer segment contents of many phototransduction proteins, particularly those of lower abundances. The goal of this study was to address this knowledge gap.

Nearly all existing information on protein amounts in the outer segment was obtained from either semi-quantitative measurements of individual or small sets of proteins (e.g. [8, 9]) or rough estimates from large proteomic datasets based on relative representations of peptide spectral counts [10]. Accordingly, there is a great disparity across published abundances for many of these proteins (e.g. [11] vs. [12] or [13] vs. [14]; see also Table 1 below). A more accurate mass spectrometry-based approach for absolute protein quantification involves the use of commercially synthesized isotope labeled peptide standards corresponding to tryptic fragments of a protein of interest. To our knowledge, this technique has only been applied to quantifying a handful of outer segment proteins in a single study [15]. The limited use of this approach is due, at least in part, to the high costs of labeled peptide standards, potential issues with the stability and solubility of these peptides and the fact that concentrations of many commercial peptide standards are not easy to independently verify in a quantitatively consistent manner [16].

These limitations have been overcome with the introduction of a strategy for absolute protein quantification using the digest of a single recombinant protein built as a concatemer of tryptic peptide standards [17, 18]. This cost-efficient approach does not require synthesizing individual peptide standards and allows to quantify multiple proteins in a single analysis. In this study, we employed a variation of this approach, termed “MS Western” [19], in which sequences of several tryptic peptides from each protein of interest are cloned in tandem as a part of a single DNA construct that also encodes several tryptic peptides from BSA. This chimeric protein is expressed in an *E. coli* strain auxotrophic for arginine and lysine grown in a medium containing heavy isotope labeled lysine and arginine. A tryptic digest of this heavy isotope labeled protein produces an equimolar set of its constituent peptides, including those from BSA. The chimeric protein is digested alongside unlabeled BSA of known amount and the sample of interest. The resulting peptide mixture is analyzed by LC-MS/MS and the absolute amounts of heavy isotope labeled BSA peptides from the chimera are determined by comparison to the corresponding peptides from unlabeled BSA whose precise amount is known. Because all other labeled peptides in the chimeric protein digest are equimolar to labeled BSA peptides, these labeled peptides can be used as standards for determining absolute (molar) amounts of each corresponding protein in the unlabeled sample of interest. This methodology has been successfully applied to the quantification of core histones in zebrafish embryogenesis [19], large sets of proteins in the *Drosophila* eye [20, 21] and central carbon metabolic enzymes in *C. elegans* [22, 23].

Using this approach, we determined the absolute abundances of twenty proteins supporting the function and structure of the mouse rod outer segment. The precision of the method was assessed by measuring the molar ratios amongst individual protein subunits from three constitutive protein complexes of well-established subunit stoichiometry. Strikingly,

the deviation from known stoichiometric ratios did not exceed 7%, which highlights the exceptional precision of this method. This enabled us to establish a precise molar ratio amongst all analyzed proteins and to calculate their absolute amounts in each outer segment. These findings resolve multiple discrepancies in the literature regarding the abundances of some of these proteins and provide new quantitative information about the membrane flippase ATP8A2 whose abundance had not yet been analyzed.

Experimental Procedures

Animal husbandry.

Animal maintenance and experiments were approved by the Duke Institutional Animal Care and Use Committee. We used C57BL/6J (Jackson Labs stock #000664) mice of both sexes between the ages of 1 and 6 months.

Composition, expression and digestion of the chimeric protein.

The polypeptide sequence of the chimeric protein, templated from [19], is illustrated schematically in Supplementary Fig. 1. It contained an N-terminal twin-strep-tag with a 3C protease cleavage site, concatenated sequences of 110 peptides (104 from proteins of interest and 6 from BSA; Supplementary Table 1), and a C-terminal His_6-tag, although we did not need to use either tag for purification. DNA encoding this construct was custom synthesized and cloned into the pET11 vector at Genscript. It was transformed into competent ΔLys, ΔArg auxotrophic *E. coli* cells [24] generated and provided by Ronald Hay (University of Dundee). Transformed cells were grown in MDAG medium supplemented with ampicillin and $^{15}N_4$,$^{13}C_6$-Arg and $^{15}N_2$,$^{13}C_6$-Lys (Cambridge Isotope Laboratory). At OD600=0.6, cells were induced with 1 mM IPTG for 4 h. Cell lysates from 50 µl of cell culture were subjected to SDS-PAGE on a 10% gel. The protein band representing the chimeric protein was cut from the gel and cleaved using a standard in-gel trypsin digestion protocol [25]. The incorporation of $^{15}N_4$,$^{13}C_6$-Arginine and $^{15}N_2$,$^{13}C_6$-Lysine was 99.5% as judged by a ratio between the intensities of unlabeled and labeled peptides in a protein expressed in heavy isotope containing medium.

Preparation and digestion of mouse rod outer segments.

Mice were dark-adapted overnight and osmotically intact rod outer segments were isolated under dim red light following a protocol adapted from [26] with modifications described in [27]. Rhodopsin concentration in the resulting preparation was measured by differential spectroscopy at 500 nm as described in [28]. Samples containing 20–30 pmol rhodopsin were mixed with 100–250 fmol BSA and cleaved with 1 µg trypsin/LysC mix (Promega) using the SP3 beads protocol described in [29].

Mass spectrometry.

The combined digest of outer segments and BSA was mixed with 100–250 fmol of the chimeric protein digest and injected into a Symmetry C18 trap column (5 µm, 180 µm×20 mm) (Waters) in 1% acetonitrile in water at 5 µl/min. The analytical separation was subsequently performed using an HSS T3 column (1.8 µm, 75 µm×200 mm) (Waters) over 90 min at a flow rate of 0.3 µl/min at 50°C. The 5–30% mobile phase B gradient

was used, where phase A was 0.1% formic acid in water and phase B was 0.1% formic acid in acetonitrile. Peptides separated by LC were introduced into the Q Exactive HF tandem mass spectrometer (Thermo Fisher Scientific) using positive electrospray ionization at 2 kV and ion transfer capillary temperature of 275°C. MS1 spectra were acquired in data-dependent acquisition (DDA) mode with the target mass resolution of 60,000 (*m/z* 200; FWHM); *m/z* range of 350–1350; target AGC value of 1×10^6; RF-lens set at 30%; and maximum injection time of 50 ms. Advanced peak detection and internal calibration (EIC) were enabled. Peptide precursor ions were selected for MS/MS using charge state filtering (z = 2 to 5); monoisotopic peak detection and dynamic exclusion time of 20 sec with mass tolerance of 10 ppm. HCD FT MS/MS was performed under normalized collision energy (NCE) of 30%; AGC target value of 5×10^4; maximum injection time of 100 ms; isolation width of precursor ions of 1.6 Th. DDA was guided by the inclusion list containing *m/z* of doubly and triply charged precursors of peptides used in subsequent absolute quantification.

Data processing.

For absolute protein quantification, raw mass spectral data files (.raw) were imported into Progenesis QI for Proteomics 4.2 software (Nonlinear Dynamics) for duplicate runs alignment of each preparation and peak area calculations. Peptides were identified using Mascot version 2.5.1 (Matrix Science) for searching a mouse UniProt 2019 reviewed database containing 17,008 entrees and the BSA sequence. Mascot search parameters were: 10 ppm mass tolerance for precursor ions; 0.025 Da for fragments mass tolerance; no missed cleavage allowed; fixed modification: carbamidomethylation of cysteine; variable modifications were oxidized methionine and N/Q deamidation and ICAT Lys_8, Arg_{10} for isotope labels. False discovery rate for protein identification was set to <1%. Only peptides with ion scores more than 25 were included in quantification. To account for variations in experimental conditions in individual LC-MS/MS runs, the integrated peak area for each identified peptide was corrected using normalization to all proteins by a Progenesis algorithm equalizing the total intensities for all peaks in each run.

Experimental design and statistical rationale.

We analyzed a total of six independently obtained rod outer segment preparations. Each sample was run in duplicate and corresponding labeled and unlabeled peptide pairs were identified by Mascot software using “SILAC K+8, R+10” variable modification. The integrated areas of peptide peaks representing XIC of full isotope cluster were averaged between duplicates. The absolute amounts of heavy isotope labeled standards from the digest of the chimeric protein were determined using reference BSA peptides, whose abundance was compared with corresponding peptides produced by tryptic cleavage of BSA standard with the exactly known concentration. Next, the amounts of unlabeled peptides representing proteins of interest were determined based on their ratios to the amounts of labeled peptide standards. The amounts of proteins were calculated by averaging the amounts of their constituent peptides, after applying the exclusion criterion described in Results. The amounts of low abundant proteins were corrected for the presence of an impurity of non-labeled amino acids in the heavy isotope labeled chimeric protein standard. This impurity, identified to represent 0.5% of the added chimeric protein was subtracted from the calculated amount of the target protein. The data for each protein were averaged

across all six outer segment preparations. Coefficient of variation was calculated using Excel.

Results

The goal of this study was to determine the absolute amounts of proteins that perform phototransduction or otherwise uniquely reside in the photoreceptor disc membranes where phototransduction takes place. We only included proteins that were documented to produce at least two unique tryptic peptides confidently identified by mass spectrometry in our previous studies [15, 27, 30, 31]. This allowed us to analyze 16 proteins directly engaged in phototransduction (entries 1–16 in Supplementary Table 1) and four additional disc-specific proteins (entries 17–20). The roles of these proteins in photoreceptor function are illustrated schematically in Fig. 1. The four remaining phototransduction proteins (PDE6γ, Gγ_1, GCAP1 and GCAP2) and the disc-specific protein PRCD were excluded from this study, as each yield only one tryptic peptide suitable for quantification.

For absolute quantification of most proteins of interest we were able to select 5 unique tryptic peptides (Supplementary Table 1) that have been consistently identified in our previous mass spectrometry studies [15, 27, 30, 31]. When possible, we excluded peptides containing methionine, tryptophan and cysteine due to a variable extent of their oxidation, as well as peptides with N-terminal aspartic acid due to a potentially decreased rate of trypsin cleavage at the Lys/Arg-Asp bond. The only protein that was represented by less than 5 peptides was the visual pigment rhodopsin, which yields only two tryptic peptides that are suitable for quantification.

To generate the chimeric protein standard, we cloned the sequences of these peptides in tandem as shown in Supplementary Fig. 1. Because rhodopsin is by far the most abundant protein in the outer segment, we included four copies of each of the two rhodopsin peptides in the chimera. This allowed us to keep the ratio between labeled and unlabeled rhodopsin peptides closer to the range for peptides representing other proteins and was accounted for in the final quantification. Behind the peptides representing outer segment proteins, we cloned 6 proteotypic peptides from BSA that were used in the original study describing the MS Western methodology[19]. The resulting construct also contained an N-terminal twin-strep-tag and 3C protease cleavage site and a C-terminal His_6-tag that were parts of the original plasmid described in [19], but not utilized in the present study. This plasmid encoded a chimeric protein with a calculated molecular mass of 143 kDa. It was expressed in ΔLys, ΔArg auxotrophic *E. coli* [24] grown in the presence of $^{13}C_6$, $^{15}N_2$ lysine and $^{13}C_6$ and $^{15}N_4$ arginine. The band corresponding to this heavy isotope labeled chimeric protein was cut out of a Coomassie-stained SDS-PAGE gel (Fig. 2A) and trypsinized using a conventional in-gel digestion protocol [25].

Our workflow for quantifying outer segment proteins is illustrated in Fig. 2B. We prepared a lysate of purified mouse rod outer segments, mixed it with BSA of known amount and trypsinized the mixture on SP3 beads as in [29]. Next, we supplemented this digest with the digest of the chimeric protein containing heavy isotope labeled peptide standards. We used a concentration of peptide standards corresponding to the middle of the concentration

range for analyzed peptides. This workflow was modified from the original MS Western protocol, in which proteins in the sample, chimera and BSA were co-digested in-gel. The advantage of this modification was that the chimera was purified by SDS-PAGE and was not contaminated by truncated fragments and/or products of incomplete translation [33]. The concentration of The resulting sample was analyzed by LC-MS/MS in two technical repeats. The analysis was performed for six independently obtained outer segment preparations.

Whereas our peptide selection aimed to avoid common issues complicating analysis, such as oxidation or incomplete digestion, we could not predict whether any of these peptides would be differentially modified in (or unevenly recovered from) outer segment vs. *E. coli* lysates, thereby compromising their quantification. To determine whether any such peptides should be excluded from the final protein quantification, we used an approach described in [19], which was applied independently to the analysis of each of the six outer segment preparations. For each of the peptides representing a given protein of interest, we calculated the fraction of ion intensity that this peptide contributes to the total ion intensity of all peptides representing that protein. This was done separately for unlabeled and heavy isotope labeled peptide sets. If a pair of unlabeled and labeled peptides is equally digested and neither is modified, their relative abundances should be close to one another. This was the case for the majority of peptides, such as for all peptides representing RGS9 in the experiment illustrated in Fig. 3A. The peptides not satisfying this criterion, either in individual experiments or systematically across all experiments, were excluded from the analysis. The examples include one peptide representing $G\beta_1$ (Fig. 3B) or two peptides representing peripherin-2 (Fig. 3C). The total number of systematically excluded peptides was six (they are labeled in red in Supplementary Table 1).

We next quantified the absolute amounts of all 20 proteins of interest (Supplementary Tables 2-7). Because it is customary to describe the contents of outer segment proteins as molar ratios to rhodopsin, we calculated these ratios for all proteins (Table 1; see also Supplementary Table 8 for statistical analysis). We also calculated the number of molecules of each protein present in a single rod outer segment. This could be derived from the molar ratio of each protein to rhodopsin because the number of rhodopsin molecules per rod outer segment is known to be between 50 and 70 million [54, 55]. We used the average value of 60 million rhodopsin molecules per outer segment in this calculation. Finally, we estimated the abundance of each protein in the space within the outer segment occupied by a single photoreceptor disc, using an average value of ~800 discs per mouse rod outer segment [56]. These estimates are summarized in Table 1, as well.

The analysis of phototransduction proteins provides a unique opportunity to assess the precision of absolute protein quantification using our methodology. Seven of the twenty proteins quantified in our study exist as constitutive multi-subunit protein complexes. The subunit stoichiometry of each of these complexes has been established by multiple independent approaches, including solved 3D structures, and can be used as a benchmark for validating the accuracy of protein quantification performed in our study. Furthermore, none of the proteins comprising these complexes are expressed in free form or as parts of other complexes. The first complex was the constitutive PDE6α/β dimer [57], for which our data deviated from the expected 1:1 stoichiometry by ~6.8%. The second was the GTPase

activating complex containing equimolar amounts of its three constituent subunits, RGS9, Gβ5 and R9AP [58]. Our measured amounts of each of these subunits were very close among themselves and differed from the expected 1:1:1 stoichiometry by only ~2.8%. The third was the tetrameric cyclic nucleotide gated (CNG) channel that has a 3:1 molar ratio between CNGα1 and CNGβ1 [59–61]. We measured the ratio between these subunits to be 3.06 :1, which differs from the theoretical value by a remarkable 1%. These calculations illustrate the exceptional precision of the analysis employed in our study and suggest that this analysis provides the most accurate quantification of multiple outer segment proteins performed to date.

Discussion

In this study, we report a precise molar ratio amongst the proteins comprising the phototransduction pathway and several other proteins supporting phototransduction in outer segment disc membranes. Remarkably, we were able to simultaneously quantify, in a single experiment, proteins whose outer segment abundances vary by three to four orders of magnitude.

Methodological considerations

The approach employed in our study was modified from the original MS Western protein quantification method [19]. While the original protocol involved SDS-PAGE and in-gel digestion of the biological sample, chimeric protein and BSA standard, we only used SDS-PAGE and in-gel digestion for the chimeric protein. This was critical to ensure that the full-length chimeric protein was free from contaminations by its under-expressed or truncated fragments. In contrast, outer segment proteins and BSA were trypsinized on beads and, subsequently, combined with the digest of the chimera. Clearly, this modification did not affect the accuracy of quantification, yet it allowed us to use the same chimeric protein digest in multiple experiments. Another advance was to adjust the number of peptide copies in the chimera in accordance with the expected abundance of quantified proteins, in our case rhodopsin. This simplified the simultaneous quantification of multiple proteins of various abundances by easing the dynamic range requirements. Overall, the success of our study shows that MS Western is a versatile protein quantification tool that allows for a great flexibility in sample preparation.

We should note that the current study is the second to report a simultaneous quantitative assessment of multiple photoreceptor outer segment proteins. The previous analysis was part of a study describing the proteomes of whole and fractionated rod outer segments [10], which included the Absolute Protein Expression (APEX) approach that is based on the assumption that the frequency of peptide identification for a given protein is directly proportional to its abundance [62]. However, the authors of [10] noted that the molar ratios amongst many proteins suggested by APEX were far from independently established values. For example, the ratio between PDE6 and rhodopsin was calculated to be an order of magnitude higher than the previously reported range [34, 37–39], while the amount of the CNG channel was about the same as PDE6 despite being known to be less abundant [46]. These and other examples in [10]

illustrate that APEX may provide only rough estimates of relative protein abundances. For this reason, we did not include the APEX values from [10] in Table 1 to avoid confusion.

Quantification of phototransduction proteins

We will now relate our current data on outer segment protein abundances to previously published values (Table 1), starting with the proteins responsible for activation of the phototransduction cascade: rhodopsin, transducin (G_t) and PDE6 (shown at the upper disc in Fig. 1B). We determined that the outer segment contents of the α and β subunits of G_t are essentially equimolar, which is consistent with these subunits being a part of a functional αβγ heterotrimer [63]. Both G_t subunits are present at an ~1:8 molar ratio to rhodopsin, which matches previous measurements in mammalian rods based on semi-quantitative Western blotting [34, 35]. Similarly, our ~1:140 ratio between the catalytic subunits of PDE6 and rhodopsin falls within the range of reported values [34, 37–39].

Another group of proteins, shown at the middle disc in Fig. 1B, is involved in deactivation of the phototransduction cascade. Rhodopsin is deactivated through phosphorylation by GRK1 (*aka* rhodopsin kinase), followed by arrestin binding to phosphorylated rhodopsin; the activity of GRK1 is regulated by the Ca^{2+}-binding protein, recoverin [1]. The published estimates of the molar ratio between GRK1 and rhodopsin range widely from 1:360 [13] to 1:40 [14]. We now show that this ratio is ~1:200. The cases of recoverin and arrestin are more complex because light causes a major redistribution of these proteins between the outer segment and the cell body [64]. The reported ratio between recoverin and rhodopsin in dark-adapted mouse rod outer segments is 1:104 [44], which is confirmed by our measured ratio of 1:111. The molar ratio between arrestin and rhodopsin in isolated dark-adapted mouse rod outer segments was reported to be within the range of 1:7 to 1:10, based on semi-quantitative Western blotting [42]. However, another study analyzing the arrestin content in tangential serial sections from a frozen flat-mounted retina argued that the upper limit of arrestin content in dark-adapted outer segments is ~7% of its total cellular amount, which corresponded to an ~1:18 molar ratio to rhodopsin [43]. We now show that this ratio is actually equal to 1:18.

Also involved in deactivation of the phototransduction cascade is the GTPase activating complex for G_t, which is a constitutive trimer of RGS9, Gβ5 and R9AP [58]. As discussed above, our experiments yielded an exceptional consistency in determining the outer segment abundances of these subunits averaging at an ~1:460 molar ratio to rhodopsin. Previous estimates ranged widely between 1:270 and 1:1,640 [11, 12, 38], and the current value falls approximately in the middle of the range from the two most recent reports [12, 38].

The next two proteins, the CNG channel and the $Na^+/K^+/Ca^{2+}$ exchanger (NCKX1), reside in the plasma membrane enclosing the outer segment (Fig. 1B). They are involved in the generation and regulation of the photoreceptor's electrical response to light [65]. The functional CNG channel in rods is a constitutive tetramer containing three CNGα1 and one CNGβ1 subunits. Our measurements corroborated this 3:1 stoichiometry nearly perfectly and showed that the tetrameric channel is present at an ~1:990 molar ratio to rhodopsin, which is an approximately twice lower content than estimated previously [46]. We also found that NCKX1 is present at an ~1:470 ratio to rhodopsin, which is about twice higher

than previously reported [47] and twice higher than the amount of the CNG channel. The CNG channel and NCKX1 exchanger have been shown to form a supramolecular complex in rods [66–69], and it has been suggested that two molecules of NCKX1 are bound to a single heterotetrameric CNG channel [68]. Our currently measured stoichiometry is entirely consistent with the latter model.

Two other proteins directly involved in generating the visual signal are the isoforms of guanylyl cyclase, GC1 and GC2, responsible for synthesizing cGMP, the second messenger in phototransduction. We show that they are present at ~1:530 and ~1:3,500 molar ratios to rhodopsin, respectively. The abundance of GC1 falls roughly in the middle of the previously reported range [8, 9, 48], while GC2 is ~2-fold more abundant than previously reported [9, 49]. Notably these enzymes are regulated by the Ca^{2+}-binding proteins, GCAP1 and GCAP2 [70], however neither GCAP1 nor GCAP2 produces a sufficient number of tryptic peptides for quantification.

Quantification of other disc-specific proteins

Peripherin-2 and ROM1 are two homologous proteins which interact to form very large oligomeric structures that fortify photoreceptor disc rims [71] (see lower disc in Fig. 1B). A recent cryo-electron tomography study [72] showed that three continuous oligomeric chains of peripherin-2/ROM1 molecules span the entire circumference of a disc rim. Based on *in vitro* analyses of proteins solubilized from disc membranes, it is widely accepted that peripherin-2 and ROM1 form homo- and hetero-tetramers that are thought to serve as the base structural units of these oligomeric chains [71]. It has been reported that peripherin-2 is ~2–2.5-fold more abundant than ROM1 [73, 74], which is well corroborated by our current data indicating that outer segments contain ~2.0-fold more peripherin-2 than ROM1. We further showed that the molar ratio between peripherin-2/ROM1 monomers and rhodopsin is ~1:12.7. An early estimate suggested that the presumed peripherin-2/ROM1 tetramers are present at an ~1:90 molar ratio to rhodopsin [50]. A different value of ~1:25 was recently calculated [51] based on fitting the dimensions of peripherin-2/ROM1 unit structures resolved by cryo-electron tomography [72] into the circumference of the disc membrane, while assuming that these units were tetramers. This would correspond to an ~1:6.3 molar ratio between peripherin-2/ROM1 monomers and rhodopsin, which is a 2-fold higher abundance than our measured value.

However, there is a possibility to reconcile our measurement with the calculation in [51]. The cryo-electron tomography in [72], which served as the basis of that calculation, did not have sufficient resolution to determine whether the peripherin-2/ROM1 structural units observed in disc rims were dimers or tetramers, while the calculation was made with the assumption that these structures were tetramers. Yet, a recent study [75] reported a pseudo-atomic resolution model of peripherin-2/ROM1 complexes suggesting that this structural unit is a dimer. In this case, the calculation in [51] would have to be adjusted by a factor of two, which would bring it to ~1:12.5 and match our current value of ~1:12.7. Because our directly measured value corresponds to the model describing the base structural units of peripherin-2/ROM1 as dimers rather than tetramers, it is likely that the structural units resolved by cryo-electron tomography are actually dimers.

The last two analyzed proteins are the lipid flippases, ABCA4 and ATP8A2, uniquely expressed in discs (Fig. 1B, lower disc). Our measured 1:790 ratio between ABCA4 and rhodopsin is notably lower than previous measurements with mammalian rods, ranging from 1:120 [36] to 1:302 [15]. The outer segment content of ATP8A2 has only been assessed as being <0.1% of the total outer segment protein [53]. We now report that it is present at an ~1:13,200 ratio with rhodopsin, which makes it the least abundant protein analyzed in our study.

Concluding remarks

To better appreciate our findings, we illustrate the distribution and abundances of membrane-associated proteins quantified in this study in a cartoon representing one quarter of one lamellar surface of a photoreceptor disc (Fig. 4). In this illustration, each protein is represented by an object of unique shape and color, and the number of these objects corresponds to the exact number of protein molecules located in this space.

One immediate observation is that the outer segment protein material is dominated by rhodopsin, which serves both as the light receptor and the essential building block of disc membranes. Our measurements indicate that rhodopsin represents an ~92.2% molar fraction of all transmembrane proteins in the disc. The next most abundant are peripherin-2 and ROM1, which together represent ~7.2% of the transmembrane protein fraction. The combined molar fraction of all other transmembrane proteins in disc membranes, including R9AP, GC1, GC2, ABCA4 and ATP8A2, account for only a meager ~0.6%. Indeed, knockout of either rhodopsin or peripherin-2 completely abolishes disc formation [76, 77]. In contrast, the knockouts of R9AP, GC1, GC2, ABCA4 or ATP8A2 cause primarily functional defects in photoreceptors [78–81]. Therefore, a mature disc is essentially built from two structural protein elements: rhodopsin within the disc lamella and peripherin-2/ROM1 in the disc rim.

The second most abundant protein in the outer segment is transducin, which is peripherally associated with disc membranes. Its high concentration at the disc surface ensures a high frequency of interactions with light-activated rhodopsin, which is required for a rapid propagation of the visual signal. Another abundant outer segment protein is arrestin, which is present in an amount sufficient to deactivate the large fraction of rhodopsin activated by a bright light stimulus. The rest of the proteins analyzed in this study are expressed in catalytic amounts. Taken together, these findings contribute to our understanding of how the phototransduction pathway functions as a single, well-coordinated molecular ensemble in the spatial constraints of the outer segment architecture.

Supplementary Material

Refer to Web version on PubMed Central for supplementary material.

Acknowledgements:

This work was supported by the NIH grants EY030451 (VYA), EY005722 (VYA), EY033763 (TRL), the Career-Starter Research Grant from the Knights Templar Eye Foundation (WJS) and Unrestricted grant to Duke University by Research to Prevent Blindness. The authors thank Ronald Hay (University of Dundee) for providing the ΔLys, ΔArg auxotrophic strain of *E. coli*. We are grateful for Dr. Aliona Bogdanova (MPI of Molecular Cell Biology and Genetics, Dresden) for expert technical support.

Data availability:

Mass spectrometry data have been deposited to the MassIVE server at Center for Computational Mass Spectrometry University of California, San Diego, MSV000090885. URL – https://massive.ucsd.edu/ProteoSAFe/dataset.jsp?task=7cca166439ed4d58bf1f392742c547e0.

References

(1). Arshavsky VY; Burns ME Photoreceptor signaling: Supporting vision across a wide range of light intensities. J Biol Chem 2012, 287 (3), 1620–1626. [PubMed: 22074925]

(2). Lamb TD Photoreceptor physiology and evolution: cellular and molecular basis of rod and cone phototransduction. J Physiol 2022, 600, 4585–4601. [PubMed: 35412676]

(3). Lamb TD; Pugh EN Jr. A quantitative account of the activation steps involved in phototransduction in amphibian photoreceptors. J Physiol 1992, 449, 719–758. [PubMed: 1326052]

(4). Astakhova LA; Firsov ML; Govardovskii VI Kinetics of turn-offs of frog rod phototransduction cascade. J Gen Physiol 2008, 132 (5), 587–604. [PubMed: 18955597]

(5). Gross OP; Pugh EN Jr.; Burns ME Calcium feedback to cGMP synthesis strongly attenuates single-photon responses driven by long rhodopsin lifetimes. Neuron 2012, 76 (2), 370–382. [PubMed: 23083739]

(6). Shen L; Caruso G; Bisegna P; Andreucci D; Gurevich VV; Hamm HE; DiBenedetto E Dynamics of mouse rod phototransduction and its sensitivity to variation of key parameters. Iet Syst Biol 2010, 4 (1), 12–32. [PubMed: 20001089]

(7). Caruso G; Klaus CJ; Hamm HE; Gurevich VV; Makino CL; DiBenedetto E Position of rhodopsin photoisomerization on the disk surface confers variability to the rising phase of the single photon response in vertebrate rod photoreceptors. Plos One 2020, 15 (10), e0240527. [PubMed: 33052986]

(8). Hwang JY; Lange C; Helten A; Hoppner-Heitmann D; Duda T; Sharma RK; Koch KW Regulatory modes of rod outer segment membrane guanylate cyclase differ in catalytic efficiency and Ca(2+)-sensitivity. Eur J Biochem 2003, 270 (18), 3814–3821. [PubMed: 12950265]

(9). Peshenko IV; Olshevskaya EV; Savchenko AB; Karan S; Palczewski K; Baehr W; Dizhoor AM Enzymatic properties and regulation of the native isozymes of retinal membrane guanylyl cyclase (RetGC) from mouse photoreceptors. Biochemistry 2011, 50 (25), 5590–5600. [PubMed: 21598940]

(10). Kwok MC; Holopainen JM; Molday LL; Foster LJ; Molday RS Proteomics of photoreceptor outer segments identifies a subset of SNARE and Rab proteins implicated in membrane vesicle trafficking and fusion. Mol Cell Proteomics 2008, 7 (6), 1053–1066. [PubMed: 18245078]

(11). He W; Cowan CW; Wensel TG RGS9, a GTPase accelerator for phototransduction. Neuron 1998, 20 (1), 95–102. [PubMed: 9459445]

(12). Martemyanov KA; Krispel CM; Lishko PV; Burns ME; Arshavsky VY Functional comparison of RGS9 splice isoforms in a living cell. Proc Natl Acad Sci U S A 2008, 105 (52), 20988–20993. [PubMed: 19098104]

(13). Sitaramayya A Rhodopsin kinase prepared from bovine rod disk membranes quenches light activation of cGMP phosphodiesterase in a reconstituted system. Biochemistry 1986, 25 (19), 5460–5468. [PubMed: 3022791]

(14). Chen CK; Woodruff ML; Chen FS; Chen Y; Cilluffo MC; Tranchina D; Fain GL Modulation of mouse rod response decay by rhodopsin kinase and recoverin. J Neurosci 2012, 32 (45), 15998–16006. [PubMed: 23136436]

(15). Skiba NP; Cady MA; Molday L; Han JYS; Lewis TR; Spencer WJ; Thompson WJ; Hiles S; Philp NJ; Molday RS; Arshavsky VY TMEM67, TMEM237, and embigin in complex with monocarboxylate transporter MCT1 are unique components of the photoreceptor outer segment plasma membrane. Mol Cell Proteomics 2021, 20, 100088. [PubMed: 33933680]

(16). Shuford CM; Walters JJ; Holland PM; Sreenivasan U; Askari N; Ray K; Grant RP Absolute protein quantification by mass spectrometry: Not as simple as advertised. Anal Chem 2017, 89 (14), 7406–7415. [PubMed: 28605192]

(17). Pratt JM; Simpson DM; Doherty MK; Rivers J; Gaskell SJ; Beynon RJ Multiplexed absolute quantification for proteomics using concatenated signature peptides encoded by QconCAT genes. Nat Protoc 2006, 1 (2), 1029–1043. [PubMed: 17406340]

(18). Beynon RJ; Doherty MK; Pratt JM; Gaskell SJ Multiplexed absolute quantification in proteomics using artificial QCAT proteins of concatenated signature peptides. Nat Methods 2005, 2 (8), 587–589. [PubMed: 16094383]

(19). Kumar M; Joseph SR; Augsburg M; Bogdanova A; Drechsel D; Vastenhouw NL; Buchholz F; Gentzel M; Shevchenko A MS Western, a method of multiplexed absolute protein quantification is a practical alternative to Western blotting. Mol Cell Proteomics 2018, 17 (2), 384–396. [PubMed: 29192002]

(20). Raghuraman BK; Hebbar S; Kumar M; Moon H; Henry I; Knust E; Shevchenko A Absolute quantification of proteins in the eye of Drosophila melanogaster. Proteomics 2020, 20 (23), e1900049. [PubMed: 32663363]

(21). Kumar M; Has C; Lam-Kamath K; Ayciriex S; Dewett D; Bashir M; Poupault C; Schuhmann K; Knittelfelder O; Raghuraman BK; Ahrends R; Rister J; Shevchenko A Vitamin A deficiency alters the phototransduction machinery and distinct non-vision-specific pathways in the Drosophila eye proteome. Biomolecules 2022, 12 (8), 1083. [PubMed: 36008977]

(22). Penkov S; Raghuraman BK; Erkut C; Oertel J; Galli R; Ackerman EJM; Vorkel D; Verbavatz JM; Koch E; Fahmy K; Shevchenko A; Kurzchalia TV A metabolic switch regulates the transition between growth and diapause in C. elegans. BMC Biol 2020, 18 (1), 31. [PubMed: 32188449]

(23). Kaptan D; Penkov S; Zhang X; Gade VR; Raghuraman BK; Galli R; Sampaio JL; Haase R; Koch E; Shevchenko A; Zaburdaev V; Kurzchalia TV Exogenous ethanol induces a metabolic switch that prolongs the survival of Caenorhabditis elegans dauer larva and enhances its resistance to desiccation. Aging Cell 2020, 19 (10), e13214. [PubMed: 32898317]

(24). Matic I; Jaffray EG; Oxenham SK; Groves MJ; Barratt CL; Tauro S; Stanley-Wall NR; Hay RT Absolute SILAC-compatible expression strain allows Sumo-2 copy number determination in clinical samples. J Proteome Res 2011, 10 (10), 4869–4875. [PubMed: 21830832]

(25). Shevchenko A; Tomas H; Havlis J; Olsen JV; Mann M In-gel digestion for mass spectrometric characterization of proteins and proteomes. Nat Protoc 2006, 1 (6), 2856–2860. [PubMed: 17406544]

(26). Tsang SH; Burns ME; Calvert PD; Gouras P; Baylor DA; Goff SP; Arshavsky VY Role for the target enzyme in deactivation of photoreceptor G protein in vivo. Science 1998, 282 (5386), 117–121. [PubMed: 9756475]

(27). Spencer WJ; Lewis TR; Phan S; Cady MA; Serebrovskaya EO; Schneider NF; Kim KY; Cameron LA; Skiba NP; Ellisman MH; Arshavsky VY Photoreceptor disc membranes are formed through an Arp2/3-dependent lamellipodium-like mechanism. Proc Natl Acad Sci U S A 2019, 116, 27043–27052. [PubMed: 31843915]

(28). Bownds D; Gordon-Walker A; Gaide-Huguenin AC; Robinson W Characterization and analysis of frog photoreceptor membranes. J Gen Physiol 1971, 58 (3), 225–237. [PubMed: 4255372]

(29). Hughes CS; Foehr S; Garfield DA; Furlong EE; Steinmetz LM; Krijgsveld J Ultrasensitive proteome analysis using paramagnetic bead technology. Mol Syst Biol 2014, 10, 757. [PubMed: 25358341]

(30). Skiba NP; Spencer WJ; Salinas RY; Lieu EC; Thompson JW; Arshavsky VY Proteomic identification of unique photoreceptor disc components reveals the presence of PRCD, a protein linked to retinal degeneration. J Proteome Res 2013, 12 (6), 3010–3018. [PubMed: 23672200]

(31). Reidel B; Thompson JW; Farsiu S; Moseley MA; Skiba NP; Arshavsky VY Proteomic profiling of a layered tissue reveals unique glycolytic specializations of photoreceptor cells. Mol Cell Proteomics 2011, 10 (3), 10.1074/mcp.M1110.002469.

(32). Burns ME; Arshavsky VY Beyond counting photons: trials and trends in vertebrate visual transduction. Neuron 2005, 48 (3), 387–401. [PubMed: 16269358]

(33). Rzagalinski I; Bogdanova A; Raghuraman BK; Geertsma ER; Hersemann L; Ziemssen T; Shevchenko A FastCAT accelerates absolute quantification of proteins using multiple short nonpurified chimeric standards. J Proteome Res 2022, 21 (6), 1408–1417. [PubMed: 35561006]

(34). Kuhn H Interactions of rod cell-proteins with the disk membrane - Influence of light, ionic-strength, and nucleotides. Curr Top Membr Trans 1981, 15, 171–201.

(35). Lobanova ES; Finkelstein S; Herrmann R; Chen YM; Kessler C; Michaud NA; Trieu LH; Strissel KJ; Burns ME; Arshavsky VY Transducin γ-subunit sets expression levels of α- and β-subunits and is crucial for rod viability. J Neurosci 2008, 28 (13), 3510–3520. [PubMed: 18367617]

(36). Hamm HE; Bownds MD Protein complement of rod outer segments of frog retina. Biochemistry 1986, 25 (16), 4512–4523. [PubMed: 3021191]

(37). Baehr W; Devlin MJ; Applebury ML Isolation and characterization of cGMP phosphodiesterase from bovine rod outer segments. J Biol Chem 1979, 254 (22), 11669–11677. [PubMed: 227876]

(38). Zhang X; Wensel TG; Kraft TW GTPase regulators and photoresponses in cones of the eastern chipmunk. J Neurosci 2003, 23 (4), 1287–1297. [PubMed: 12598617]

(39). Pentia DC; Hosier S; Cote RH The glutamic acid-rich protein-2 (GARP2) is a high affinity rod photoreceptor phosphodiesterase (PDE6)-binding protein that modulates its catalytic properties. J Biol Chem 2006, 281 (9), 5500–5505. [PubMed: 16407240]

(40). Dumke CL; Arshavsky VY; Calvert PD; Bownds MD; Pugh EN Jr. Rod outer segment structure influences the apparent kinetic parameters of cyclic GMP phosphodiesterase. J Gen Physiol 1994, 103 (6), 1071–1098. [PubMed: 7931138]

(41). Cote RH; Brunnock MA Intracellular cGMP concentration in rod photoreceptors is regulated by binding to high and moderate affinity cGMP binding sites. J Biol Chem 1993, 268 (23), 17190–17198. [PubMed: 8394335]

(42). Song X; Vishnivetskiy SA; Seo J; Chen J; Gurevich EV; Gurevich VV Arrestin-1 expression level in rods: balancing functional performance and photoreceptor health. Neuroscience 2011, 174, 37–49. [PubMed: 21075174]

(43). Strissel KJ; Sokolov M; Trieu LH; Arshavsky VY Arrestin translocation is induced at a critical threshold of visual signaling and is superstoichiometric to bleached rhodopsin. J Neurosci 2006, 26 (4), 1146–1153. [PubMed: 16436601]

(44). Strissel KJ; Lishko PV; Trieu LH; Kennedy MJ; Hurley JB; Arshavsky VY Recoverin undergoes light-dependent intracellular translocation in rod photoreceptors. J Biol Chem 2005, 280 (32), 29250–29255. [PubMed: 15961391]

(45). Klenchin VA; Calvert PD; Bownds MD Inhibition of rhodopsin kinase by recoverin. Further evidence for a negative feedback system in phototransduction. J Biol Chem 1995, 270 (27), 16147–16152. [PubMed: 7608179]

(46). Cook NJ; Hanke W; Kaupp UB Identification, purification, and functional reconstitution of the cyclic GMP-dependent channel from rod photoreceptors. Proc Natl Acad Sci U S A 1987, 84 (2), 585–589. [PubMed: 2432613]

(47). Cook NJ; Kaupp UB Solubilization, purification, and reconstitution of the sodium-calcium exchanger from bovine retinal rod outer segments. J Biol Chem 1988, 263 (23), 11382–11388. [PubMed: 2841326]

(48). Aparicio JG; Applebury ML The bovine photoreceptor outer segment guanylate cyclase: purification, kinetic properties, and molecular size. Protein Exp Purif 1995, 6 (4), 501–511.

(49). Helten A; Saftel W; Koch KW Expression level and activity profile of membrane bound guanylate cyclase type 2 in rod outer segments. J Neurochem 2007, 103 (4), 1439–1446. [PubMed: 17868328]

(50). Goldberg AF; Molday RS Subunit composition of the peripherin/rds-rom-1 disk rim complex from rod photoreceptors: hydrodynamic evidence for a tetrameric quaternary structure. Biochemistry 1996, 35 (19), 6144–6149. [PubMed: 8634257]

(51). Gulati S; Palczewski K Structural view of G protein-coupled receptor signaling in the retinal rod outer segment. Trends Biochem Sci 2022, 48 (2), 172–186. [PubMed: 36163145]

(52). Sun H; Nathans J Stargardt's ABCR is localized to the disc membrane of retinal rod outer segments. Nat Genet 1997, 17 (1), 15–16. [PubMed: 9288089]

(53). Coleman JA; Kwok MC; Molday RS Localization, purification, and functional reconstitution of the P4-ATPase Atp8a2, a phosphatidylserine flippase in photoreceptor disc membranes. J Biol Chem 2009, 284 (47), 32670–32679. [PubMed: 19778899]

(54). Lyubarsky AL; Daniele LL; Pugh EN Jr. From candelas to photoisomerizations in the mouse eye by rhodopsin bleaching in situ and the light-rearing dependence of the major components of the mouse ERG. Vis Res 2004, 44 (28), 3235–3251. [PubMed: 15535992]

(55). Nickell S; Park PS; Baumeister W; Palczewski K Three-dimensional architecture of murine rod outer segments determined by cryoelectron tomography. J Cell Biol 2007, 177 (5), 917–925. [PubMed: 17535966]

(56). Liang Y; Fotiadis D; Maeda T; Maeda A; Modzelewska A; Filipek S; Saperstein DA; Engel A; Palczewski K Rhodopsin signaling and organization in heterozygote rhodopsin knockout mice. J Biol Chem 2004, 279 (46), 48189–48196. [PubMed: 15337746]

(57). Cote RH Characteristics of photoreceptor PDE (PDE6): similarities and differences to PDE5. Int J Impot Res 2004, 16 Suppl 1, S28–33. [PubMed: 15224133]

(58). Arshavsky VY; Wensel TG Proctor Lecture. Timing is everything: GTPase regulation in phototransduction. Invest Ophthalmol Vis Sci 2013, 54, 7725–7733. [PubMed: 24265205]

(59). Weitz D; Ficek N; Kremmer E; Bauer PJ; Kaupp UB Subunit stoichiometry of the CNG channel of rod photoreceptors. Neuron 2002, 36 (5), 881–889. [PubMed: 12467591]

(60). Zheng J; Trudeau MC; Zagotta WN Rod cyclic nucleotide-gated channels have a stoichiometry of three CNGA1 subunits and one CNGB1 subunit. Neuron 2002, 36 (5), 891–896. [PubMed: 12467592]

(61). Zhong H; Molday LL; Molday RS; Yau KW The heteromeric cyclic nucleotide-gated channel adopts a 3A:1B stoichiometry. Nature 2002, 420 (6912), 193–198. [PubMed: 12432397]

(62). Lu P; Vogel C; Wang R; Yao X; Marcotte EM Absolute protein expression profiling estimates the relative contributions of transcriptional and translational regulation. Nat Biotechnol 2007, 25 (1), 117–124. [PubMed: 17187058]

(63). Arshavsky VY; Lamb TD; Pugh EN Jr. G proteins and phototransduction. Ann Rev Physiol 2002, 64, 153–187. [PubMed: 11826267]

(64). Calvert PD; Strissel KJ; Schiesser WE; Pugh EN Jr.; Arshavsky VY Light-driven translocation of signaling proteins in vertebrate photoreceptors. Trends Cell Biol 2006, 16 (11), 560–568. [PubMed: 16996267]

(65). Genovese F; Reisert J; Kefalov VJ Sensory transduction in photoreceptors and olfactory sensory neurons: Common features and distinct characteristics. Front Cell Neurosci 2021, 15, 761416. [PubMed: 34690705]

(66). Bauer PJ; Drechsler M Association of cyclic GMP-gated channels and Na(+)-Ca(2+)-K+ exchangers in bovine retinal rod outer segment plasma membranes. J Physiol 1992, 451, 109–131. [PubMed: 1328615]

(67). Poetsch A; Molday LL; Molday RS The cGMP-gated channel and related glutamic acid-rich proteins interact with peripherin-2 at the rim region of rod photoreceptor disc membranes. J Biol Chem 2001, 276 (51), 48009–48016. [PubMed: 11641407]

(68). Schwarzer A; Schauf H; Bauer PJ Binding of the cGMP-gated channel to the Na/Ca-K exchanger in rod photoreceptors. J Biol Chem 2000, 275 (18), 13448–13454. [PubMed: 10788457]

(69). Molday RS; Molday LL Molecular properties of the cGMP-gated channel of rod photoreceptors. Vis Res 1998, 38 (10), 1315–1323. [PubMed: 9666999]

(70). Dizhoor AM; Peshenko IV Regulation of retinal membrane guanylyl cyclase (RetGC) by negative calcium feedback and RD3 protein. Pflugers Arch 2021, 473 (9), 1393–1410. [PubMed: 33537894]

(71). Stuck MW; Conley SM; Naash MI PRPH2/RDS and ROM-1: Historical context, current views and future considerations. Prog Retin Eye Res 2016, 52, 47–63. [PubMed: 26773759]

(72). Poge M; Mahamid J; Imanishi SS; Plitzko JM; Palczewski K; Baumeister W Determinants shaping the nanoscale architecture of the mouse rod outer segment. Elife 2021, 10, e72817. [PubMed: 34931611]

(73). Kedzierski W; Weng J; Travis GH Analysis of the rds/peripherin.rom1 complex in transgenic photoreceptors that express a chimeric protein. J Biol Chem 1999, 274 (41), 29181–29187. [PubMed: 10506174]

(74). Loewen CJ; Molday RS Disulfide-mediated oligomerization of Peripherin/Rds and Rom-1 in photoreceptor disk membranes. Implications for photoreceptor outer segment morphogenesis and degeneration. J Biol Chem 2000, 275 (8), 5370–5378. [PubMed: 10681511]

(75). El Mazouni D; Gros P Cryo-EM structures of peripherin-2 and ROM1 suggest multiple roles in photoreceptor membrane morphogenesis. Sci Adv 2022, 8 (45), eadd3677. [PubMed: 36351012]

(76). Humphries MM; Rancourt D; Farrar GJ; Kenna P; Hazel M; Bush RA; Sieving PA; Sheils DM; McNally N; Creighton P; Erven A; Boros A; Gulya K; Capecchi MR; Humphries P Retinopathy induced in mice by targeted disruption of the rhodopsin gene. Nat Genet 1997, 15 (2), 216–219. [PubMed: 9020854]

(77). Cohen AI Some cytological and initial biochemical observations on photoreceptors in retinas of rds mice. Invest Ophthalmol Vis Sci 1983, 24 (7), 832–843. [PubMed: 6862791]

(78). Keresztes G; Martemyanov KA; Krispel CM; Mutai H; Yoo PJ; Maison SF; Burns ME; Arshavsky VY; Heller S Absence of the RGS9.Gbeta5 GTPase-activating complex in photoreceptors of the R9AP knockout mouse. J Biol Chem 2004, 279 (3), 1581–1584. [PubMed: 14625292]

(79). Baehr W; Karan S; Maeda T; Luo DG; Li S; Bronson JD; Watt CB; Yau KW; Frederick JM; Palczewski K The function of guanylate cyclase 1 and guanylate cyclase 2 in rod and cone photoreceptors. J Biol Chem 2007, 282 (12), 8837–8847. [PubMed: 17255100]

(80). Weng J; Mata NL; Azarian SM; Tzekov RT; Birch DG; Travis GH Insights into the function of Rim protein in photoreceptors and etiology of Stargardt's disease from the phenotype in abcr knockout mice. Cell 1999, 98 (1), 13–23. [PubMed: 10412977]

(81). Coleman JA; Zhu X; Djajadi HR; Molday LL; Smith RS; Libby RT; John SW; Molday RS Phospholipid flippase ATP8A2 is required for normal visual and auditory function and photoreceptor and spiral ganglion cell survival. J Cell Sci 2014, 127 (Pt 5), 1138–1149. [PubMed: 24413176]

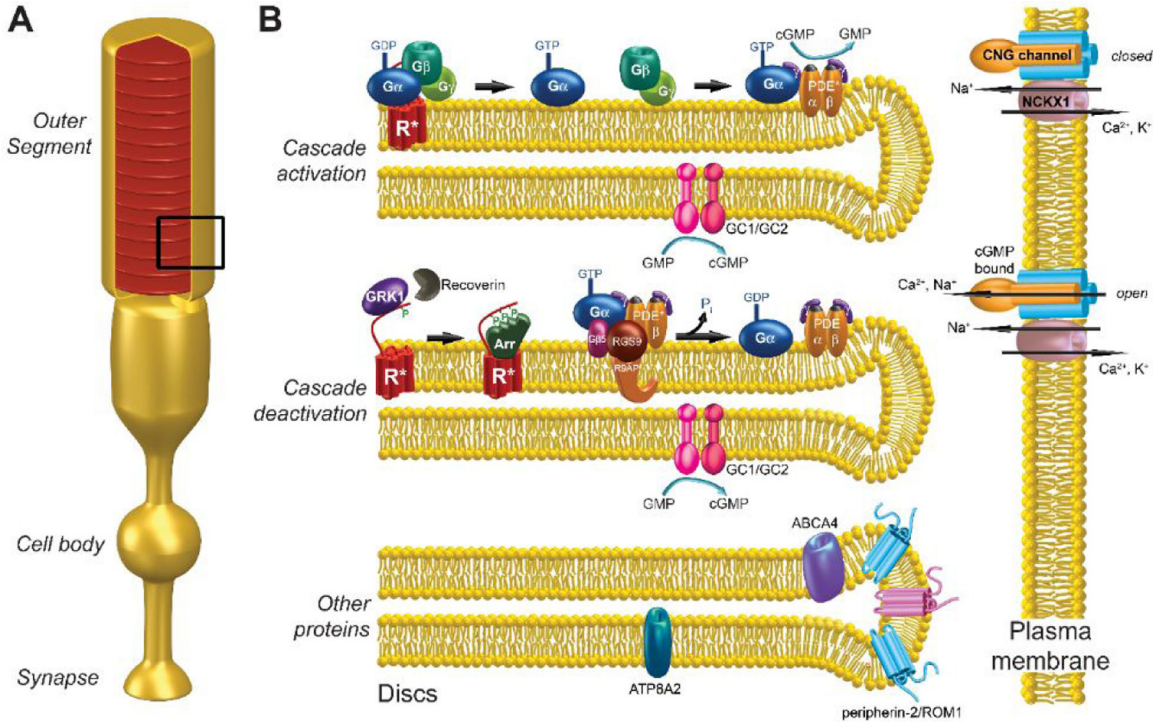

Figure 1. Cartoon illustrating localization and function of proteins analyzed in this study.

A. Schematic of a rod photoreceptor cell. **B.** Zoomed-in view of the portion of the outer segment boxed in panel A. Illustrated at the *upper disc* is the activation of the phototransduction cascade, including photoexcited rhodopsin (R*), transducin (Gα and Gβγ) and PDE6 (PDEαβγ). Two guanylyl cyclase isoforms (GC1 and GC2) responsible for cGMP synthesis are shown on the bottom membrane leaflet. Illustrated at the *middle disc* are the reactions responsible for cascade deactivation. R* is deactivated through phosphorylation by rhodopsin kinase (GRK1) and subsequent arrestin (Arr) binding; the activity of GRK1 is regulated by recoverin. Transducin deactivation occurs through GTP hydrolysis facilitated by the RGS9/Gβ5/R9AP GTPase activating complex; this returns PDE6 to its inactive state. The *plasma membrane* harbors the cGMP-gated (CNG) channel containing three α and one β subunits. This channel is open in the dark and closes upon cascade activation by light. The same membrane harbors the $Na^+/K^+/Ca^{2+}$ exchanger (NCKX1). Illustrated at the *lower disc* are two tetraspanin proteins (peripherin-2 and ROM1) fortifying the disc rim and two lipid flippases (ABCA4 and ATP8A2). The drawing is modified with permission from [32].

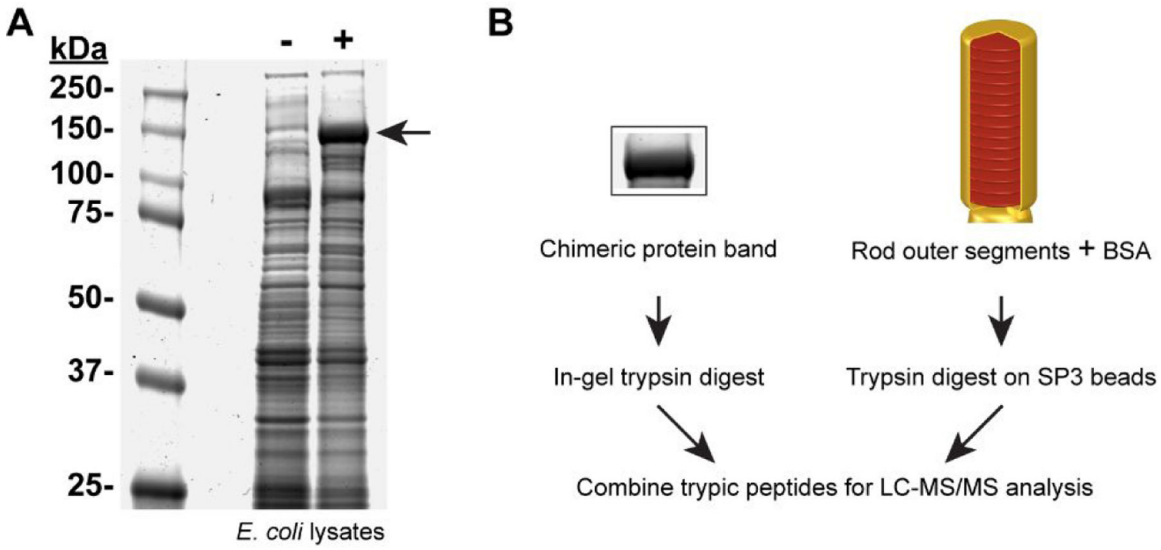

Figure 2. Experimental workflow for absolute quantification of outer segment proteins.

A. Coomassie-stained SDS-PAGE gel of *E. coli* lysates (50 μl) from uninduced (−) and IPTG-induced (+) cells transformed with the DNA construct encoding the chimeric protein. Induction with IPTG caused a high level of expression of the chimeric protein migrating at the predicted molecular mass of ~143 kDa (arrow). **B.** General experimental workflow for absolute quantification of outer segment proteins. A preparation of rod outer segments was combined with a known amount of BSA and digested with trypsin on SP3 beads. In parallel, the ~143 kDa chimeric protein band was cut out from the Coomassie-stained SDS-PAGE gel and underwent in-gel trypsin digestion. The two digests were combined and subjected to LC-MS/MS analysis.

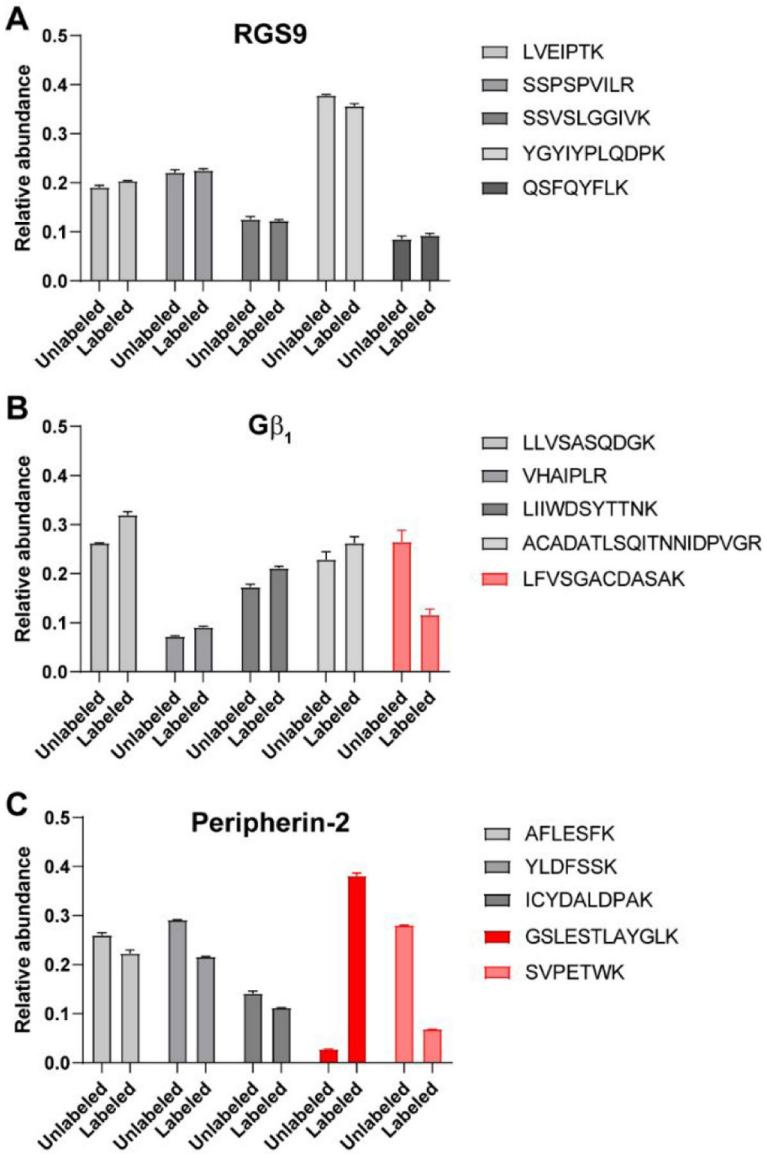

Figure 3. Peptide selection for final protein quantification.

For each peptide representing a protein shown in each panel, the fraction of ion intensity that this peptide contributes to the total ion intensity of all peptides representing this protein was calculated separately for unlabeled and heavy isotope labeled peptide sets. **A.** Relative abundances of unlabeled and labeled peptides representing RGS9 in a single experiment with technical duplicates. In this case, the relative abundances of each unlabeled and the corresponding labeled peptide matched closely and satisfied the inclusion criterion. **B.** Relative abundances of unlabeled and labeled peptides representing $G\beta_1$. The relative abundances of one unlabeled and labeled peptide pair (shown in red) were >2-fold different. The other four peptide pairs satisfied the inclusion criterion. **C.** Relative abundances of unlabeled and labeled peptides representing peripherin-2. The relative abundances of two unlabeled and labeled peptide pairs were >2-fold different. The other three peptide pairs satisfied the inclusion criterion.

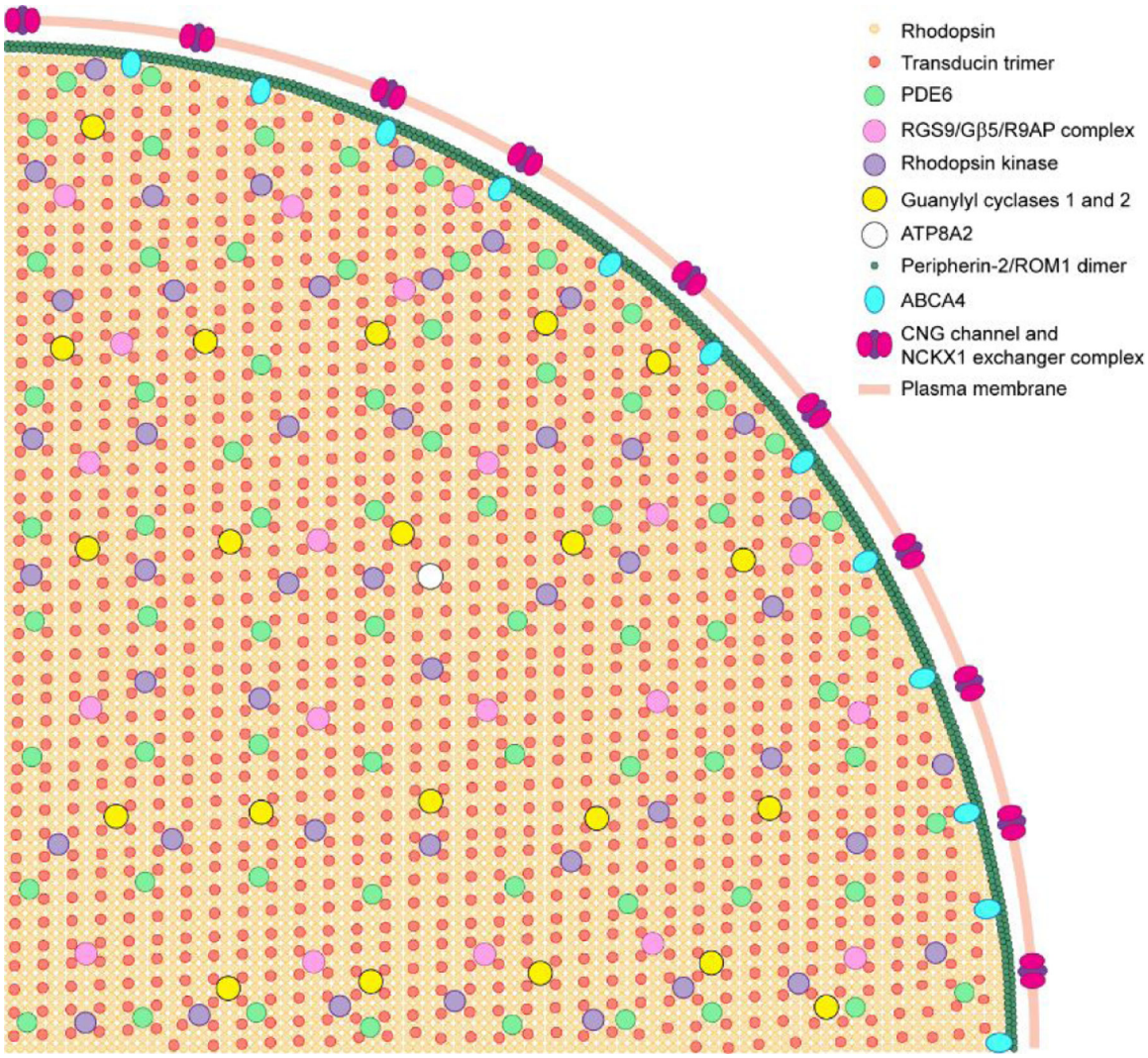

Figure 4. Cartoon illustrating the amounts of proteins in a section of the photoreceptor disc.

The drawing shows the exact number of molecules for membrane proteins analyzed in this study within the space of one quarter of a photoreceptor disc. Shown is one disc surface and the corresponding portion of the outer segment plasma membrane surrounding this disc. The symbols representing each protein are specified in the figure. Symbol sizes do not reflect the actual dimensions of the proteins they represent; rather, less abundant proteins are shown as larger symbols for ease of visualization. Whereas plasma membrane shares many proteins with discs, only the plasma membrane specific CNG channel and NCKX1 are shown at this membrane. The peripherin-2/ROM1 structural units are shown as dimers as suggested by recent ultrastructural analyses described in the text.

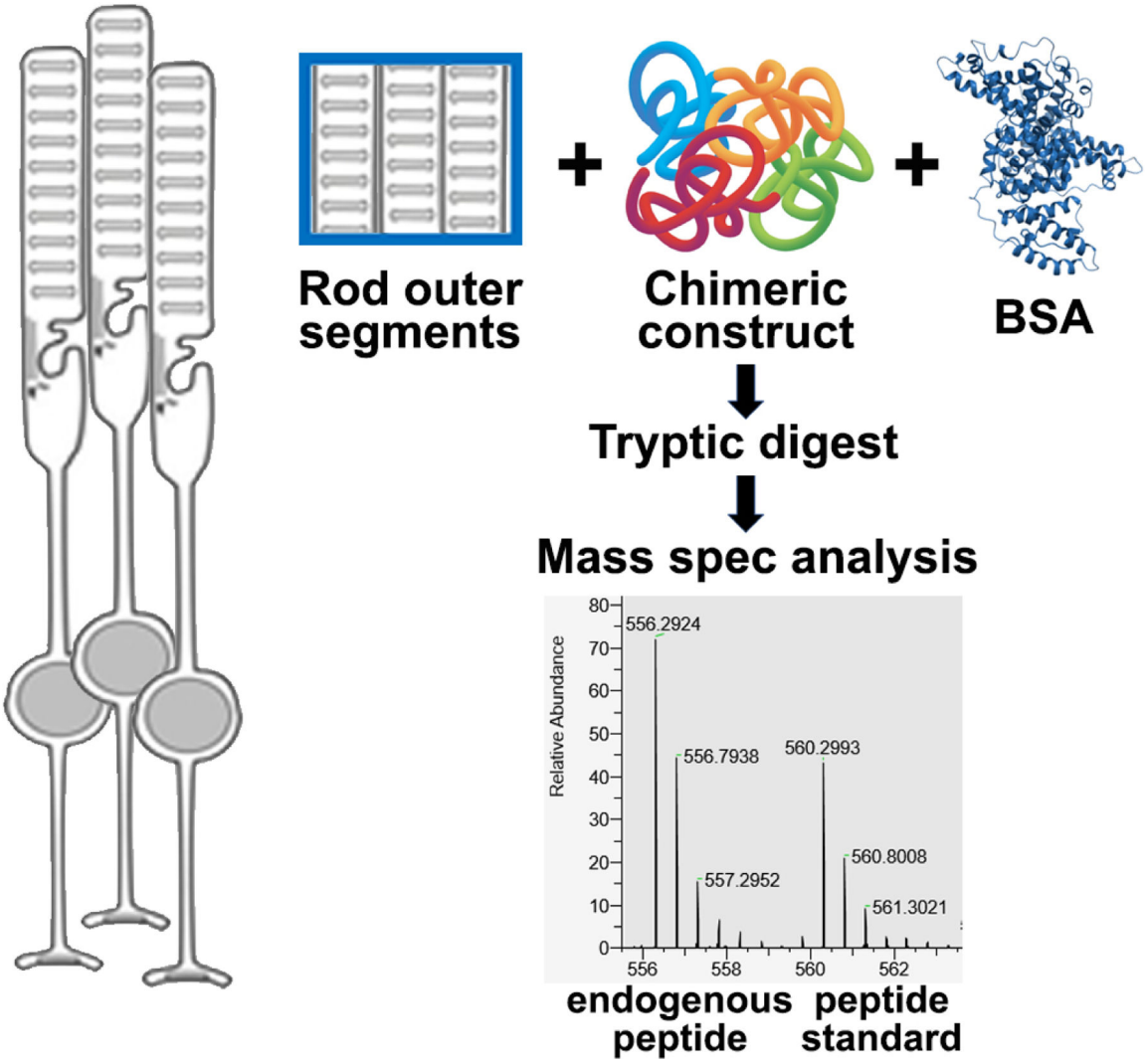

Table 1.
Summary of protein quantification in dark-adapted mouse rod outer segments

Protein	Ratio to rhodopsin[1]	Coefficient of variation, %	Molecules per rod outer segment	Molecules per disc	Reported ratio to rhodopsin
Rhodopsin	-	-	60,000,000[2]	75,000	-
$G\alpha_t$	1:7.8	2.9	7,690,000	9,600	1:8 [34]; 1:8 [35]; 1:12 [26]; 1:8 *[36]
$G\beta_1$	1:7.9	2.2	7,590,000	9,500	1:8 [34]; 1:6 [35], 1:12 [26] 1:10 *[36]
PDE6α	1:132	6.6	455,000	570	1:120 [34]; 1:40–170 [37]; 1:65–104 [38]; 1:310 [39]; 1:200 *[36], 1:270 *[40]; 1:330 *[41]
PDE6β	1:141	8.4	426,000	530	
GRK1	1:201	8.9	299,000	370	1:360 [13]; 1:40 [14]
Arrestin	1:18	12	3,340,000	4,200	1:7–10 [42]; ≤1:18 [43]; 1:33 *[36]
Recoverin	1:111	27	541,000	670	1:104 [44]; 1:174 *[45]
RGS9	1:461	5.8	130,000	170	1:1,640 [11]; 1:610–1:910 [38]; 1:269 [12]
Gβ5	1:469	6.2	128,000	160	
R9AP	1:474	9.6	127,000	160	
CNGα1[3]	1:323	6.2	185,000	230	~1:500 for the tetrameric channel [46]
CNGβ1[3]	1:988	9.2	60,700	76	
NCKX1	1:472	7.4	127,000	160	1:800 [47]
Guanylyl cyclase 1	1:526	8.1	114,000	140	1:440 [48]; 1:260 [8]; 1:1,400 [9]
Guanylyl cyclase 2	1:3,490	7.2	17,200	21	1:6,600 [49]; 1:5,800 [9]
Peripherin-2	1:19	8.9	3,160,000	3,900	1:90 for the peripherin-2/ROM1 tetramer [50]; calculated as 1:25 for the tetramer [51]
ROM1	1:39	6.0	1,540,000	1,900	
ABCA4	1:794	5.2	75,600	95	1:302 [15], 1:120 [52], 1:167 *[36]
ATP8A2	1:13,150	11	4,560	8	<0.1% of total outer segment protein [53]

*These values were determined for frog rather than mammalian outer segments.

[1]Data are averaged from six biological replicates (see Supplementary Table 8 for detailed statistical information).

[2]This value for rhodopsin is averaged from 54, 55.

[3]The molar ratio to rhodopsin is calculated to be 1:966 for the tetrameric CNG channel.